Cretaceous Research 38 (2012) 80–96

Contents lists available at SciVerse ScienceDirect

Cretaceous Research

journal homepage: www.elsevier.com/locate/CretRes

Nannofossil biostratigraphy, strontium and carbon isotope stratigraphy, cyclostratigraphy and an astronomically calibrated duration of the Late Campanian *Radotruncana calcarata* Zone

Michael Wagreich[a,*], Johann Hohenegger[b], Stephanie Neuhuber[a]

[a] University of Vienna, Department of Geodynamics and Sedimentology, Althanstrasse 14, 1090 Wien, Austria
[b] University of Vienna, Institute of Paleontology, Althanstrasse 14, 1090 Wien, Austria

ARTICLE INFO

Article history:
Received 20 July 2011
Accepted in revised form 12 April 2012
Available online 16 May 2012

Keywords:
Campanian
Cyclostratigraphy
Calcarata Zone
Nannofossil
Carbon stable isotopes

ABSTRACT

A section from the southern (Austro-Alpine Northern Calcareous Alps) margin of the Penninic Ocean in the NW Tethys realm of Late Campanian age is investigated stratigraphically. Plankton foraminifer and nannofossil biostratigraphy designate the presence of the *Globotruncana ventricosa* Zone and the *Radotruncana* (*Globotruncanita*) *calcarata* Zone, and standard nannofossil zones CC21–UC15c^{TP} and CC22ab–UC15de^{TP}. The combination of carbon isotope stratigraphy, strontium isotopes, and cyclostratigraphy allows a detailed chronostratigraphic correlation. Periodicity was obtained by power spectral analysis, sinusoidal regression, and Morlet wavelets. The duration of the *calcarata* Total Range Zone is calculated by orbital cyclicity expressed in thickness data of limestone–marl rhythmites and stable carbon isotope data. Precessional, obliquity, and short and long eccentricity cycles are identified and give an extent of c. 806 kyr for the zone. Mean sediment accumulation rates are as low as 1.99 cm/kyr and correspond well to sediment accumulation rates in similar settings. We further discuss chronostratigraphic implications of our data.

1. Introduction

The Campanian represents a significant time interval during the Late Cretaceous climate change from the mid-Cretaceous maximum greenhouse mode to a moderate greenhouse mode of the earth climate system during the Late Cretaceous (e.g., Huber et al., 2002). During this Cretaceous long-term evolution, short-term climatic and environmental events become more and more recognized (e.g., Jenkyns, 2003; Wagreich et al., 2011). A significant cooling trend was reconstructed for the Campanian (e.g., Li et al., 1999) and the highest provincialism in terms of calcareous nannofossil assemblages was recognized during this time interval (Burnett, 1998). Quantification and modeling of climate and paleoceanographic events and the evaluation of their significance to recent global climate change depends on accurate and precise timing. Astronomical dating provides a base for such timing on a (floating) astronomical scale (for a recent overview see Hinnov and Ogg, 2007).

The Campanian stage was introduced by d'Orbigny in 1852 based on typical successions in the Champagne of France (for historical overview see, e.g., Ogg et al., 2004). The modern definition using GSSPs (Global Boundary Stratotype Section and Point) is based on a proposed GSSP for the base of the Campanian at Ten Mile Creek, Texas, USA (Gale et al., 2008; see also Wagreich et al., 2009b) and the base of the Maastrichtian (i.e. the top of the Campanian) at Tercis le Lande, France (Odin and Lamaurelle, 2001, with numerous references therein). Due to the longevity of the Campanian (12.9 Myr according to Ogg et al., 2004), complete rock records of the stage are rare, and, consequently, complete cyclic records are missing, although in parts of the Campanian the applicability of cyclostratigraphy and astrochronology has been already documented, i.e. Herbert et al. (1999), Hennebert et al. (2009), Neuhuber and Wagreich (2009), Robaszynski and Mzoughi (2010), and Voigt and Schönfeld (2010).

We focus on a particular part of the Late Campanian, the *Radotruncana* (*Globotruncanita*) *calcarata* Planktonic Foraminifer Zone (*calcarata* Zone in the following), and correlate this zone to nannofossil biostratigraphy. The analyzed cyclic record from the Eastern Alps of Austria allows a floating astrochronology, and gives an accurate estimate for the duration of this zone. We compare this data to other records such as stable isotopes and strontium isotopes, and correlate the TRZ of *Radotruncana (Globotruncanita) calcarata* within and outside the Tethyan realm.

* Corresponding author. Tel.: +43 1 4277 53465; fax: +43 1 4277 9534.
E-mail address: michael.wagreich@univie.ac.at (M. Wagreich).

0195-6671/$ – see front matter © 2012 Elsevier Ltd. All rights reserved.
doi:10.1016/j.cretres.2012.04.006

2. Geological setting and paleogeography

The Postalm section (Fig. 1) follows a mountain road from Abtenau to the Postalm alpine pasture area, at the Retschegg peak (coordinates of the base of the section WGS84 013° 23′ 11″ E; 47° 36′ 44″ N). It exposes a continuous section of reddish marly limestones and marls (CORBs, Hu et al., 2005; Wagreich and Krenmayr, 2005; see Fig. 2), the Nierental Formation, that is part of the Gosau Group of the Northern Calcareous Alps (NCA).

Sediments of the Postalm section were deposited in a pelagic to hemipelagic bathyal environment, at the southern margin of the Penninic Ocean, which is a part of the Northwestern Tethys Ocean system that connected the Tethys to the North Atlantic (Faupl and Wagreich, 2000; Wagreich et al., 2009a). The abyssal basin of the Rhenodanubian Flysch and Ultrahelvetic Units were situated to the north of the NCA (Fig. 1) (e.g., Egger and Mohammed, 2010; Neuhuber et al., 2007).

During the Late Cretaceous, the NCA, a part of the Austro-Alpine megaunit, were situated at the southern, active continental margin of the Penninic Ocean (Wagreich, 1993). The complex structural evolution of the NCA, a part of the Eastern Alps fold-and-thrust belt, includes Early Cretaceous thrusting and cover-nappe stacking, followed by subsidence of the Gosau Group basins from the Turonian onwards (Faupl and Wagreich, 2000). Oblique subduction of the Penninic Ocean below the Austro-Alpine microplate resulted in strong dextral shearing between the southern microplate and the Penninic realm. This resulted in the formation of a tectonically active, rapidly subsiding southern shelf and the formation of slope basins along the active continental margin of the Austro-Alpine microplate (Wagreich, 1993). From the Santonian onward the Upper Gosau Subgroup was deposited in such slope basins including the Campanian Nierental Formation with its deep-water pelagic and hemipelagic sediments (Wagreich and Krenmayr, 2005).

3. Methods

3.1. Sampling and sample preparation

The Postalm section comprises more than 180 m of Campanian sediments. A 31 m thick interval was logged bed-by-bed, with a total of 84 samples. This interval covers the c. 16 m thick *calcarata* Zone with a total of 60 samples. Because of the strong difference in bed thickness (see Fig. 2), no standard sample interval can be given; the mean of the sample intervals lies at 33 cm.

3.2. Biostratigraphy

The section was investigated for planktonic foraminifera and calcareous nannofossils, with special focus on the recognition of the *calcarata* Zone. Marl and marlstone samples were disintegrated with hydrogen peroxide and the tenside Rewoquad© for investigation of foraminifera, and washed over 63–150–300–600 μm sieves. The 150 μm and 300 μm size fractions were used for biostratigraphic investigation, i.e. presence or absence of *R. calcarata*. Additional thin section analysis was carried out for some of the more indurated marly limestones to characterize microfacies types and to estimate plankton abundances.

For nannofossil investigation 30 smear slides of the Postalm section were prepared using a small piece of sediment and a drop of distilled water. The sediment was smeared onto a glass slide and fixed with Canada balsam. The samples were examined qualitatively under the light microscope for nannofossil biostratigraphy without detailed quantitative evaluation. We refer to Burnett (1998) for nannofossil taxonomy (Table 1).

3.3. Carbonate and stable isotope analysis

Of each sample, subsamples were taken and ground to a fine powder in an agate mill. This powder was dried at 90 °C, homogenized and used for stable carbon and oxygen analysis and for geochemical investigation. Bulk sediment samples were analyzed for stable carbon and oxygen isotopes using a ThermoFinnigan DeltaPlusXL mass spectrometer equipped with a GasBench II following the procedure of Spötl and Vennemann (2003) at the Institute for Geology and Paleontology, University of Innsbruck. Results are calibrated against NBS 19, CO1, and CO8 standard reference materials and reported on the VPDB scale. The error of carbon isotope data is 0.02% and for oxygen isotopes 0.18%. Carbonate content was measured by acidification of 1 g sample with diluted HCl and volumetric conversion of liberated CO_2 to carbonate phases (Müller–Gastner bomb). Each sample was measured in duplicate (error range ±0.5% $CaCO_3$) and we report mean values in this article.

3.4. Strontium isotopes

Sr isotopes were analyzed at the Laboratory of Geochronology, Department of Lithospheric Research, Center for Earth Sciences,

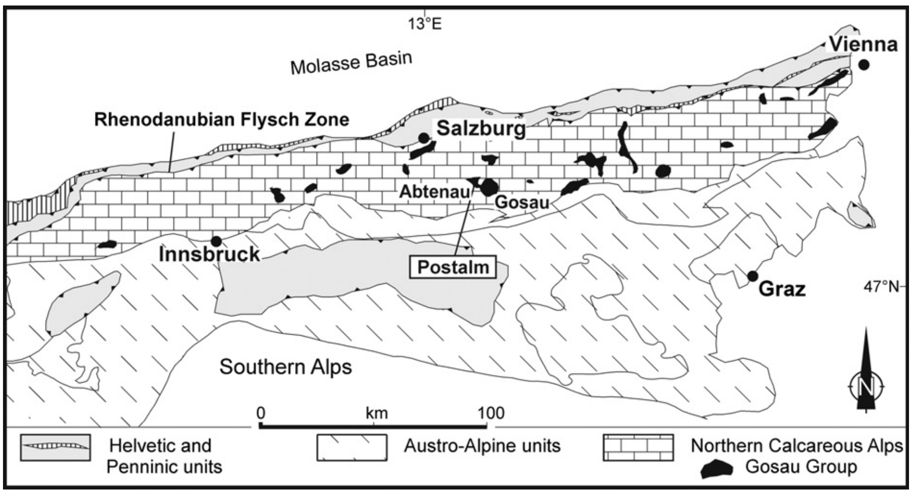

Fig. 1. Geological sketch map of the Eastern Alps including the investigated section at Postalm (Northern Calcareous Alps).

Fig. 2. Outcrop photograph of sediments of the *G. calcarata* Zone at the Postalm section from the base of the *calcarata* Zone (note the presence of distinct limestone–marl cycles; length of photograph c. 4 m).

University of Vienna. Samples were leached in different concentrations of CH_3COOH and HCl, and element separation followed conventional procedures, using an AG® 50 W-X8 (200–400 mesh, Bio-Rad) resin and HCl as elution medium. Total procedural blanks for Sr were <1 ng. Sr fractions were loaded as chlorides and vaporized from a Re double filament, using a ThermoFinnigan® Triton TI TIMS. A $^{87}Sr/^{86}Sr$ ratio of 0.710252 ± 0.000005 ($n = 4$) and 0.710245 ± 0.000003 ($n = 12$) was determined for the NBS987 (Sr) international standard during different runs, and the ratios were recalculated accordingly to a NIST 987 value of 0.710248 as recommended by McArthur et al. (2001). Within-run mass fractionation was corrected for $^{86}Sr/^{88}Sr = 0.1194$. Analytical errors of Sr isotope ratios are reported as 2σ standard deviation.

To minimize the effects of diagenesis and contamination by clay particles, the strontium isotope measurements have been performed preferably on planktonic foraminifer tests, mainly of the genus *Globotruncana*. Planktonic foraminifera are moderately preserved. Tests are filled with diagenetic calcite cement and some calcite overgrowths have been recognized. Planktonic foraminiferal tests were handpicked from washed residues, cleaned in an ultrasonic bath and leached with 1N CH_3COOH for 3 h.

3.5. Orbital cyclicity and astronomical calibration

Cyclicity was investigated using variation in thickness of limestone and marl sequences (Fig. 2). Further we related stable carbon isotope excursions to section meters. Periodicity was obtained using power spectral analysis, sinusoidal regression and Morlet wavelets (Hammer and Harper, 2006). Cross correlation based on sinusoidal regressions were introduced for the first time and cross correlations with equal and unequal intervals were calculated using programs developed by J.H. (see also Hohenegger and Wagreich, 2012). The program packages SPSS, PAST and Excel were used for common statistics.

4. Results

4.1. Foraminiferal biostratigraphy

Radotruncana (Globtruncanita) calcarata (Cushman, 1927) is a species of the globotruncanid planktonic foraminifera group. The species is regarded to belong to the genus *Radotruncana* El-Naggar, 1971 (e.g., Huber et al., 2008; Petrizzo et al., 2011), or *Globotruncanita* Reiss, 1957 (emended by Robaszynski et al., 1984) or to the genera *Globotruncana* (e.g., Robaszynski and Caron, 1995). *Radotruncana calcarata* is easily recognized by its spines (peripheral extensions of chambers along sutures by tapering tubolospines, e.g., Longoria and VonFeldt, 1991). The first description of the species was given by Cushman (1927), the last detailed taxonomic investigation of the group stems from Longoria and VonFeldt (1991).

The *Radotruncana calcarata* Zone (e.g., *Globotruncanita calcarata* Zone of Robaszynski et al., 1984; Caron, 1985; Robaszynski and Caron, 1995; Puckett and Mancini, 1998; *Globotruncana calcarata* Zone of other authors, e.g., Sigal, 1977; *R. calcarata* Zone (KS27) of ODP/IODP zonations, e.g., Premoli Silva et al., 1998, Huber et al., 2008; zone CF10 of Li et al., 1999) is a well defined, and globally used Late Cretaceous zone based on the total range of its nominate species. The *calcarata* Total Range Zone is widespread in low- to mid-latitude successions and recognized as a rather short time interval within the Late Campanian (e.g., Caron, 1985; Robaszynski and Caron, 1995; Puckett and Mancini, 1998). The relatively short taxon range of the nominate taxon led to the definition of a total range zone (e.g., Robaszynski and Caron, 1995; Puckett and Mancini, 1998).

For a long time the last occurrence (LO) of *R. calcarata*, and thus the top of the *calcarata* Total Range Zone, was interpreted to represent the base of the Maastrichtian, especially in Tethyan sections (e.g., Caron, 1985). This was corrected by Schönfeld and Burnett (1991), who recognized that the zone is well within the

Table 1
Calcareous nannofossil distribution in the Postalm section.

Zeugrhabdotus spiralis		▪			▪	▪			▪							▪					▪	
Zeugrhabdotus embergeri		▪	▪	▪		▪	▪						▪			▪	▪				▪	
Zeugrhabdotus diplogrammus		▪	▪	▪	●	▪	▪	▪	▪	▪	▪	▪	▪	▪	●	▪	▪	▪	▪	▪	▪	
Watznaueria barnesae		■	■	■	■	■	■	■	■	■	■	■	■	■	■	■	■	■	■	■	■	
Uniplanarius trifidus		▪	▪		▪	▪	▪	▪		▪	▪	▪	▪	▪	▪	▪	●	●	▪			
Uniplanarius gothicus/sissinghi		▪		▪	▪	▪		▪	▪	▪	▪	▪	▪	▪	▪	▪	▪		▪	▪	▪	
Tranolithus orionatus		▪	▪	▪	▪	▪	▪	▪	▪		▪			▪			●		▪			
Tranolithus minimus						▪	▪		▪													
Staurolithites sp.							▪									▪				▪		
Rucinolithus sp.		▪	▪			▪	▪				▪				▪							
Retecapsa crenulata		●	●	■	●	●	■	▪	▪	■	●	●	■	▪	■	●	●	●	▪	▪	▪	
Reinhardtites cf. *levis*		●	▪	▪	●	▪	▪	▪	▪	▪	▪	▪	▪		▪	▪		▪				
Reinhardtites anthophorus		▪	▪	▪	▪	▪	▪	▪	▪				▪	▪	▪		▪		▪		▪	
Quadrum sp.		▪	▪			▪	▪		▪				▪	▪	▪	▪	▪	▪	▪	▪	▪	
Prediscosphaera spinosa					▪	▪	▪					▪	▪					▪			▪	
Prediscosphaera grandis																▪						
Prediscosphaera cretacea		▪	▪	■	●	●	▪	●	▪	▪	▪	▪	▪	▪	■	●	●	■	■	■	■	
Petrarhabdus copulatus				▪		▪	▪	▪				▪		▪		▪				▪		
Operculodinella operculata																				▪	▪	
Octolithus multiplus																				▪		
Micula staurophora		●	■	●	■	▪	●	●	■	●	▪	●	■	●	■	■	●	■	●	■	■	
Micula praemurus				▪	▪	▪		▪	▪	▪					▪	▪	▪		▪			
Microrhabdulus decoratus		▪	▪	▪	▪	▪		▪	▪			▪	▪	▪	▪	▪			▪		▪	
Microrhabdulus belgicus					▪			▪														
Manivitella pemmatoidea			▪		▪		▪	▪	▪				▪									
Lucianorhabdus cayeuxii ssp. B							▪								▪	▪					▪	
Lucianorhabdus cayeuxii		●	▪	●	■	▪	▪	▪	▪	▪	▪	▪	▪	▪	■	●	●	●	▪	●	●	
Lithraphidites cf. *praequadratus*		▪																				
Lithraphidites carniolensis		▪	▪	▪	▪	▪	▪	▪	▪	▪	▪				▪	▪		▪		▪	▪	
Kamptnerius magnificus		▪		▪	▪		▪	▪					▪		▪		▪			▪	▪	
Hexalithus gorkae						▪																
Helicolithus sp.												▪										
Gartnerago sp.					▪															▪		
Eiffellithus turriseiffeli		▪	▪	▪	▪	▪	▪	▪	▪	▪	▪	▪	▪	▪	●	●	▪	▪	▪	▪	▪	
Cylindralithus sp.			▪		▪						▪	▪	▪	▪		▪	▪	▪			▪	
Cyclagelosphaera sp.							▪													▪		
Cribrosphaerella sp.					▪	▪	▪				▪		▪		▪		▪					common
Cribrosphaerella ehrenbergii		●	●	■	■	●	●	▪	▪	▪	▪	▪	▪	●	●	■	●	●	▪	■	■	■
Corollithion sp.																▪					▪	
Chiastozygus litterarius		▪	▪	▪	▪	▪	▪	▪	▪	▪	▪	▪	▪	▪	▪	●		▪	▪		▪	
Ceratolithoides sp.					▪	▪	▪													▪		
Ceratolithoides aculeus		▪	▪	▪	●	▪	▪	▪	▪	▪	●	▪	●	●	▪	▪	▪	●	▪	▪	▪	
Calculites obscurus		▪														▪		▪	▪	▪	●	few
Broinsonia parca constricta		▪	▪	▪	●	●	●	▪	▪	▪	▪	▪	▪	▪	▪	▪	▪	●	▪	▪	●	●
Broinsonia parca parca		▪	▪	▪	▪	▪	●	▪	▪	▪	▪	▪	▪	▪	▪	▪	▪	▪	▪	▪	●	
Braarudosphaera bigelowii			▪																	▪		
Biscutum cf. *magnum*					▪		▪	▪			▪	▪			▪	▪	▪	▪				
Biscutum constans		▪	▪	▪	▪	▪	▪	▪	▪	▪			▪		▪	▪		▪	▪		▪	
Arkhangelskiella cymbiformis		▪	▪	▪	▪	▪	▪	▪	▪	▪	▪	▪	▪	▪	▪	▪	▪	▪	▪	▪	▪	rare
Ahmuellerella octoradiata				▪						▪										▪	●	▪
Sample No.	**Postalm section**	08/16	08/15	08/14	08/13	08/12	08/11	08/10	08/09	08/08	08/07	08/04	08/02	08/01	07/44	07/43	07/41	07/37	07/34	07/33	07/30	
Meter in section		30.9	29.8	29.4	29.0	28.5	28.1	27.8	27.6	27.0	26.2	22.5	20.8	20.3	18.8	15.6	14.3	12.8	11.5	10.2	7.5	
Abundance		10	20	10	20	10	20	10	20	10	10	10	10	5	10	10	10	20	10	10	20	
Preservation		P	P	P	P	P	P	P	P	M	P	M	M	P	M	M	M	M	P	M	M	
UC/CC-Zones		**UC15d/CC22abc**																				
Foraminifera Zones									***calcarata***													
Chronostratigraphy		**UPPER CAMPANIAN**																				

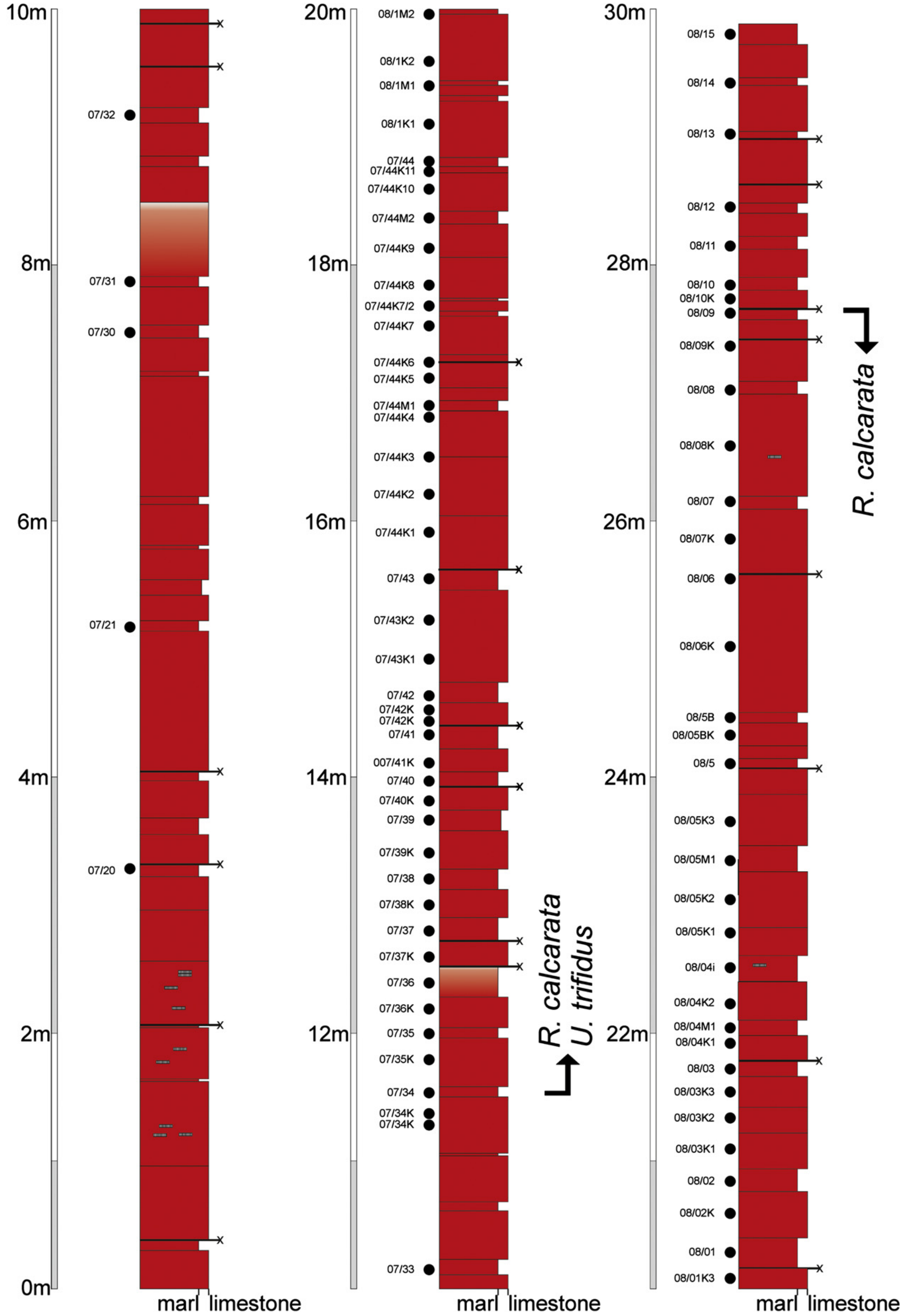

Fig. 3. Detailed log, planktonic foraminifera and nannofossil bioevents of the Postalm section around the *calcarata* Zone.

Late Campanian and far below the base of the Maastrichtian as defined by belemnites in the boreal-temperate realm. Our work identifies the *calcarata* Zone as a short time interval of less than 1 Ma within the Late Campanian (or even within the middle Campanian). However, the exact position of the *calcarata* Zone in respect to macrofossil biostratigraphic scales, the GSSP section of the Campanian–Maastrichtian boundary at Tercis, France (Odin and Lamaurelle, 2001) and the chalk sections of England and Northern Germany remains unclear or only loosely constrained by stepwise correlation with different fossil groups or chemostratigraphy. The stratigraphic position of the *calcarata* Zone within the Late Campanian ammonite zonation and its relation to the FO of the ammonite *Pachydiscus neubergicus* as a primary marker for the base of the Maastrichtian was confirmed by Ion and Odin (2001) in the Maastrichtian GSSP at Tercis (France) and correlated Spanish sections (Küchler et al., 2001). Although the presence and actual range of *R. calcarata* remains somehow dubious at Tercis, based on several differing parallel studies and the problem of thin section vs. washed sample data (compare Ion and Odin, 2001), the range in the GSSP section lateron was more secured (Odin et al., 2004; Odin, 2010).

Within the investigated part of the Postalm section *R. calcarata* starts at 11.53 m and ranges up to 27.61 m, resulting in a zonal thickness of 16.08 m (Fig. 3). Samples below that interval can be attributed to the *Globotruncana ventricosa* Zone (or *Contusotruncana plummerae* Zone of Petrizzo et al., 2011), samples above to the *Globotruncanella havanensis* Zone. The focus of this research was to identify the *calcarata* Zone and did not include a detailed survey of planktonic foraminifera.

4.2. Calcareous nannofossil biostratigraphy

Based on nannofossil marker species, the investigated section can be divided into two nannofossil standard zones (Table 1): (1) CC21 of Perch-Nielsen (1985) – UC15c^{TP} of Burnett (1998), at the Postalm section from 0 m to 11.50 m, defined by the presence of *Quadrum (Uniplanarius) sissinghii* and additional markers like *Broinsonia parca parca*, *Broinsonia parca constricta*, *Reinhardtites anthophorus*, *Reinhardtites* cf. *levis* and *Ceratolithoides aculeus*; and (2) CC22ab–UC15de^{TP}, from 11.53 m until the top of the investigated section, defined by the FO of *Uniplanarius(Quadrum) trifidus* and the continuous presence of *Reinhardtites anthophorus*. *Eiffellithus eximius*, which normally is still present in these zones (e.g., Burnett, 1998), was not found in the *calcarata* Zone of the Postalm section.

Direct correlations of nannofossils and planktic foraminifer zonations (e.g., Wagreich and Krenmayr, 1993; Gardin et al., 2001;

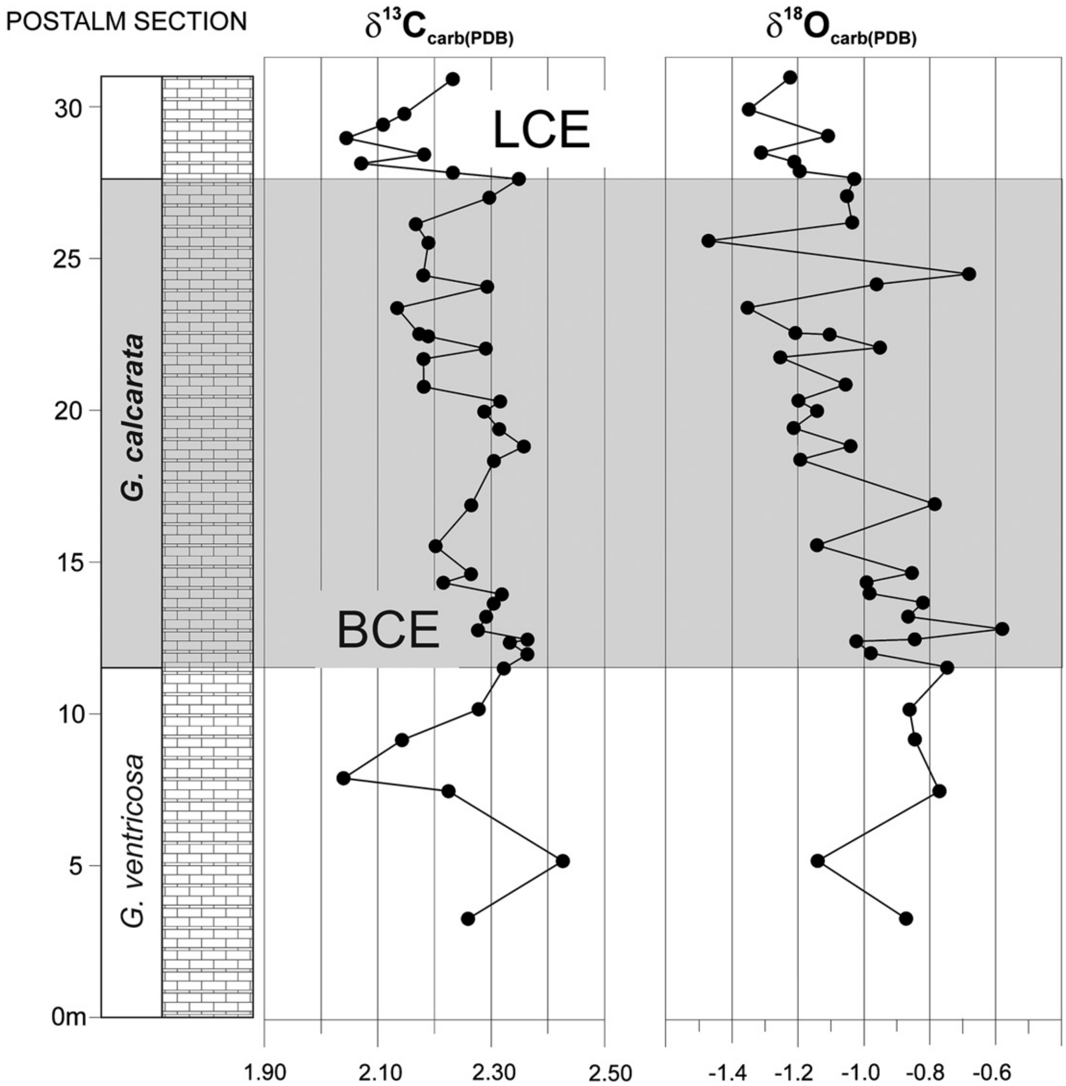

Fig. 4. Stable carbon and oxygen isotopes from marly bulk samples of the Postalm section. Tentative positions of the Late Campanian negative carbon isotope Event (LCE, Jarvis et al., 2002; Voigt et al., 2010) and the positive carbon isotope Base Calcarata Event (BCE, Wendler et al., 2011) indicated.

Küchler et al., 2001; see also Ogg et al., 2004) indicate that the FO of *R. calcarata* is roughly equivalent to or slightly above the FO of *U. trifidus*. In the investigated section the FO of *R. calcarata* and the FO of *Uniplanarius (Quadrum) trifidus* co-occur in the same sample (Fig. 3). The LO of *R. calcarata* still falls into CC22ab–UC15de^{TP}, below the LO of *Reinhardtites anthophorus* and *Eiffellithus eximius*. The data compiled by Odin and Lamaurelle (2001) on the Global Boundary Section and Stratotype (GSSP) at Tercis, southern France of the lower boundary of the Maastrichtian, indicate a fairly similar picture, although nannofossil data by several involved specialists are controversial as first and last occurrences of some nannofossil markers were placed differently in the GSSP section (see Gardin et al., 2001).

Despite a moderate to poor preservation, nannofossil assemblages are diverse with 50 taxa. Assemblages are dominated by common *Watznaueria barnesae*. Other common taxa (more than 1 specimen per field of view) include *Micula staurophora*, *Cribrosphaerella ehrenbergii*, *Lucianorhabdus cayeuxii*, *Prediscosphaera cretacea*, and *Retecapsa crenulata*. Typical low- to mid-latitude "Tethyan" nannofossils such as *Ceratolithoides aculeus*, *Uniplanarius (Quadrum) trifidus* and *Uniplanarius(Quadrum) sissinghi* besides relatively high amounts of *Watznaueria* ssp. support the Tethyan character of the nannofossil assemblage. Cooler water "boreal" species like *Kamptnerius magnificus* are rare.

4.3. Stable carbon and oxygen isotopes

Although diagenesis plays some role, largely primary values and trends are recorded in the carbon isotope values. Stable carbon isotope concentration of bulk sediments ranges in general between 2 and 2.5‰ VPDB (Fig. 4). Marly intervals are less prone to diagenetic alteration (e.g., Westphal and Munnecke, 2003) therefore we concentrate on analyses of marly lithologies. A negative excursion (minimum at 2.04‰ VPDB) below the *calcarata* Zone is followed by a first positive excursion (double peak at 2.36‰ VPDB) within the zone at 12.00–12.45 m. A negative excursion with a peak of 2.20‰ VPDB at 15.55 m and a positive excursion at 18.81 m (2.35‰ VPDB) are followed by a gradual decrease with minor wiggles and a final positive peak at the top of the *calcarata* Zone at 27.61 m (again at 2.35‰ VPDB). Above the zone a negative excursion is present at 29.02 m (2.04‰ VPDB).

Stable oxygen isotopes are – compared to carbon isotopes – more readily affected by diagenetic alteration (Anderson and Arthur, 1983) and regarded as less reliable in Alpine sections (e.g., Neuhuber et al., 2007). Bulk oxygen isotopes of marl beds of the Postalm section show a decreasing trend from values around −0.80‰ at the base of the zone to values around −1.20‰ at the top.

4.4. Strontium isotope stratigraphy

Corrected values adjusted to the NBS987 (Sr) international standard give a range of strontium isotope ratios for the *calcarata* Zone of 0.707655 ± 0.000018–0.707722 ± 0.000004 in the Postalm section (mean of 15 samples 0.707679). Slightly higher values are recorded up-section (Fig. 6), that is in accordance with the general increasing trend of strontium isotope values during the Campanian–Maastrichtian (McArthur et al., 2001; McArthur and Howarth, 2004). Some scatter in the data is present due to diagenesis. Largely similar values of 0.707667 ± 0.000009 (Gosau Valley area) and 0.707673 ± 0.000009–0.707671 ± 0.000012 (Gams basin) have also been obtained from the *calcarata* Zone in other Austrian sections (Wagreich, unpublished data).

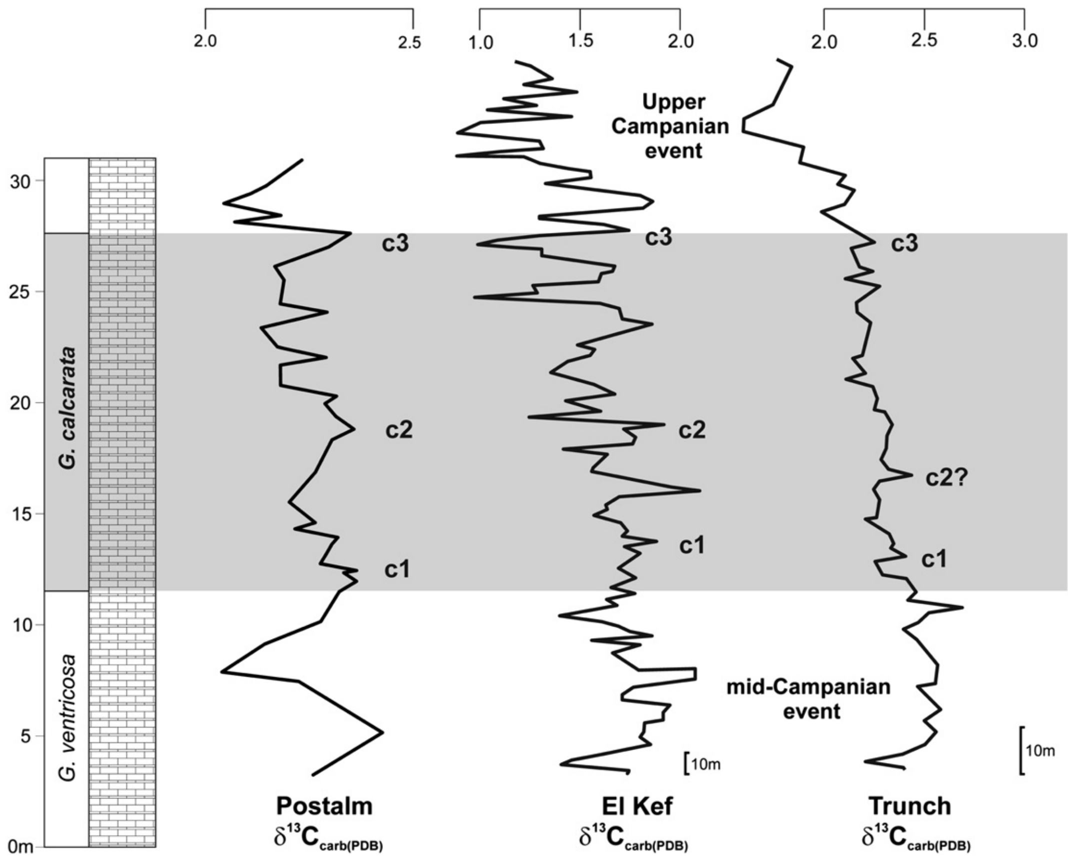

Fig. 5. Carbon isotope curves around the *calcarata* Zone from Postalm, El Kef (Tunisia, modified from Jarvis et al., 2002, to fit to equal length of the *calcarata* Zone) and Trunch (UK, modified from Jarvis et al., 2002). Note different scale of Postalm vs. El Kef and Trunch.

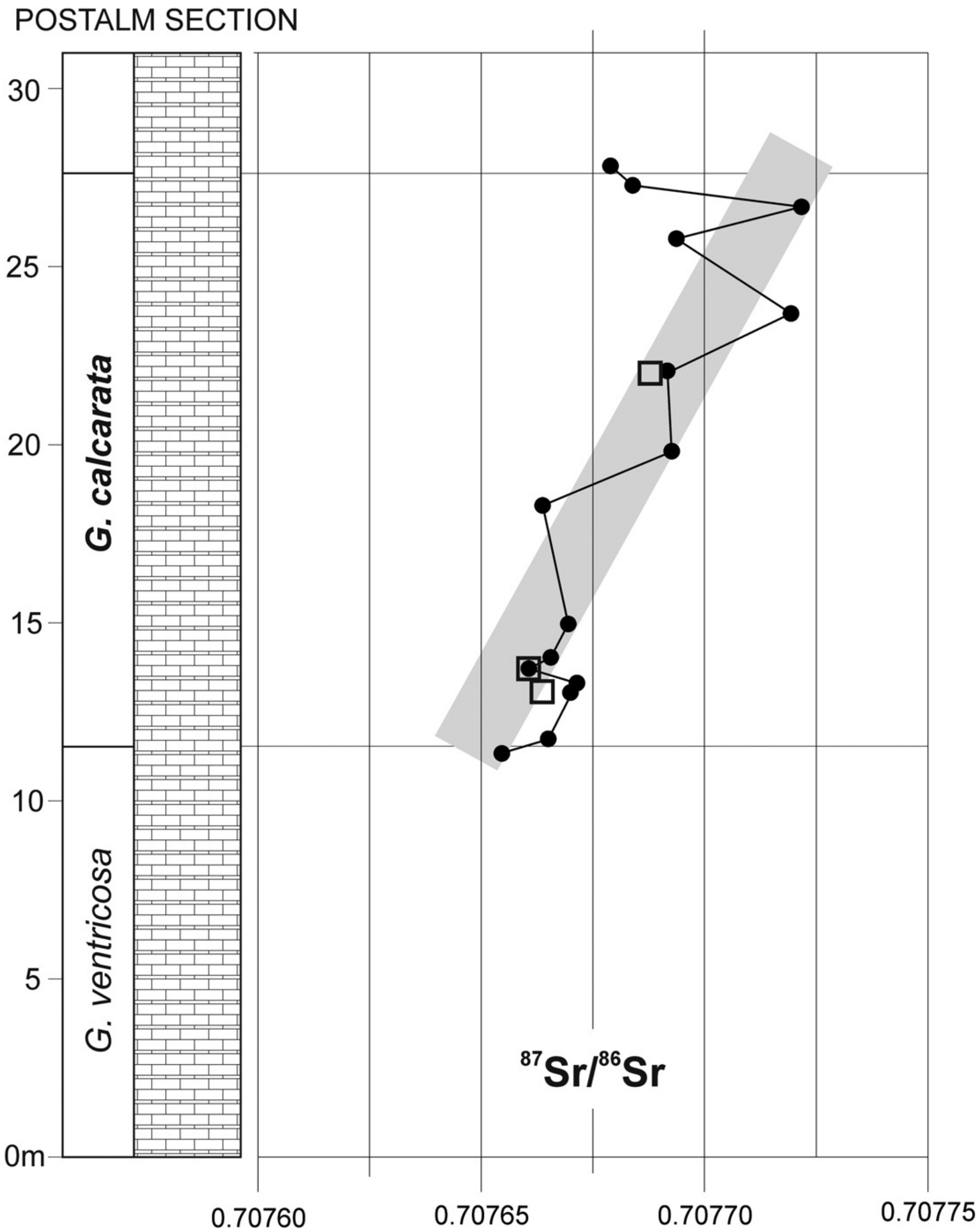

Fig. 6. Strontium isotope data of planktonic foraminifers (black circles) and inoceramid shell fragments (open squares) from the Postalm section. Gray trend line based on linear regression.

Inoceramid prisms of disarticulated inoceramid shells from the *calcarata* Zone were also measured and lie well within the range of values of foraminiferal tests (0.707653 ± 0.000019 to 0.707680 ± 0.000004).

4.5. Cyclostratigraphy

The Postalm section comprises a succession of rhythmic alternations of beds with varying carbonate content. Here, carbonate contents of slightly more indurated marly limestone beds (see Fig. 2) range from 66.4 to 75.7% $CaCO_3$ with a mean of 71.3% ($n = 42$) while marl beds have carbonate contents between 59.5 and 71.3% with a mean of 66.0% ($n = 42$). Thus, a significant overlap between the two lithotypes does exist in the carbonate contents.

Counting marl–marly limestone couplets within the range of *R. calcarata* results in c. 41 cycles $\pm$ 1 couplet. The uncertainty arises from a nearly compact interval around 16 m where no clear intervening softer marl beds are present. Faint bedding planes indicate probably the presence of three marly limestone beds within this otherwise 1.4 m thick massive interval.

Higher order cycles are not directly visible in the Postalm section (Fig. 2), although the regular thickness changes in marl and marly limestone beds indicate the presence of such cycles.

In theory, each limestone–marl alternation represents a cycle of similar duration (Agterberg and Banerjee, 1969; Schwarzacher, 1975). Accordingly, varying thickness changes of limestone and marls may represent a set of superior cycles. Although differential compaction and diagenesis may have altered the primary thickness signal to some extent, the presence of a primary signal recorded in limestone–marl couplets in the sense of Westphal et al. (2010) is evident from heterolithic fillings of burrows (*Zoophycos* and *Chondrites*-type) and from the fact that strontium isotope and carbon isotope values of bulk carbonate are well within the range of Campanian marine values.

First, we test the hypothesis if the thickness of limestones and marls in the section follow the same periodicities. Therefore both features were correlated by parametric (Pearson) and non-parametric (Spearman) tests. In both cases, the negative correlation is significant at the 5% significance level ($r_{Pearson} = -0.2033$, $p(H_0) = 0.0445$; $r_{Spearman} = -0.2198$, $p(H_0) = 0.0328$) where a thick limestone layer is almost always followed by a thin marl layer and vice versa (thin limestone layer–thick marl layer; Fig. 7).

Regarding thickness in limestone layers, the power spectral analysis resulted in several distinct, but non-significant peaks due to the low sample number ($n = 71$). Period lengths of the highest peaks are marked in Fig. 8A.

The power spectral analysis based on the thickness of marl layers shows a strong peak close to significance that corresponds to a period of 20 layers. Periods of the following 5 important peaks are shown in Fig. 8C.

Similarities are obvious comparing Morlet wavelets of limestone and marls (Fig. 9A), but the negative correlation between marls and limestones is clearly demonstrated in the alternating peaks and valleys of the larger periods. Especially at the log2 scale 4.45 (limestone) and 4.3 (marl) as well as at 3.5 (both sediments) the connection between peaks in the one sediment type and valleys in the other sediment type is visible (Fig. 9A). Additionally, this can be demonstrated in the shorter periods of sinusoidal functions based on power spectra (Fig. 9B). Regarding functions with the coincident period 5.43 (both sediments) and similar periods of 2.27 (limestone) versus 2.30 (marls), the alternation of peaks and valleys is obvious. Especially functions with the identical period of 5.44

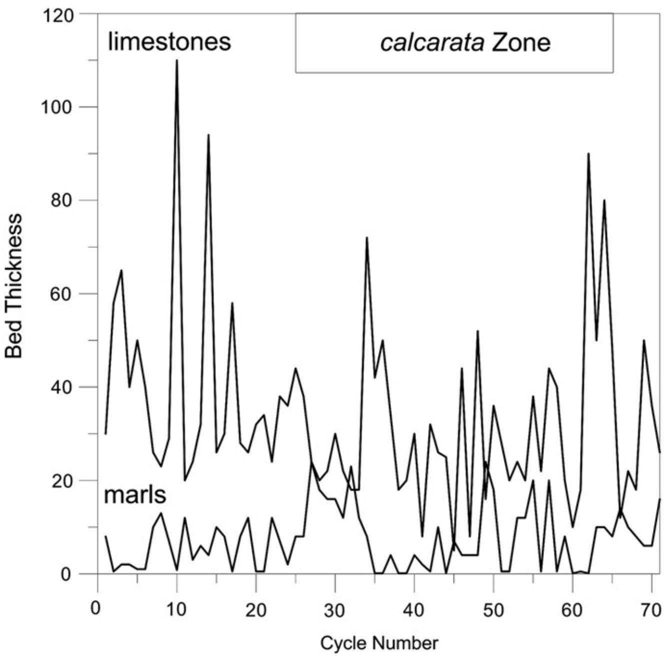

Fig. 7. Thickness data of successive limestone and marl parts of couplets, starting at cycle 1–71 of the Postalm section.

demonstrate this alternation, shifting functions against each other by half of period lengths; thus a local minimum in the one sediment type is represented by a local maximum in the other (Fig. 9B).

Comparing significant periods of power spectra between limestone and marl in the Postalm section, then two of them are very similar, even identical (2.267 versus 2.305 and 5.437 in both sediments), while the periods of 3.684 (limestone) and 3.500 (marl) slightly differ. Additionally to these concurrent periods, the period with the highest power (6.667 in limestone, 20.0 in marl) must be included to interpret their causes. The fit of empirical data in both sediment types with the above mentioned 5 overlying sinusoidal functions resulted in a significant fit for marls, while limestones are less significant because of lacking the prominent period of 70 layers. The inclusion of this cycle raises the significance in the thickness cycles of limestones remarkably, while the influence in marls is low (Fig. 10).

Stable carbon isotopes have been measured in 43 limestone samples of the Postalm section. Because of the low sample number, power spectra resulted in 5 non-significant peaks in decreasing order (Fig. 8B). Similar results could be obtained regarding the 39 marl samples in respect to stable carbon isotopes, where the coincidence between limestone and marl peaks are remarkable (6.93 v. 6.91 m, 2.99 v. 3.11 m, 1.71 v. 1.69 m and 1.27 v. 1.35 m; Fig. 8B, D).

4.5.1. Transfer into orbital cycles

In principle, the exact duration of Cretaceous orbital cycles is not identical with Neogene and recent cycle durations, because of their inconsistency in earlier periods and the chaotic nature of the system (e.g., Berger et al., 1992; Laskar et al., 2011). The eccentricity cycle of 405 kyr seems to be the single, most stable astronomical cycle that is consistent during the Paleogene and the Late Cretaceous (Berger et al., 1992; Laskar et al., 2011). Thus it can be used for fitting the duration of precession cycles based on the number of limestone–marl cycles using combined cross correlation (Hohenegger and Wagreich, 2012).

We start our analysis by assuming that a single limestone–marl cycle is caused by orbital precession of unknown time duration (e.g., Herbert et al., 1999). First, the 41 limestone–marl cycles of the *calcarata*-zone had to be transferred into increasing time segments, starting from an interval of 700 kyr based on a 17.073 kyr precession period up to 990 kyr with a period length of 24.146 kyr.

The search for the best fit of the 405 kyr eccentricity cycle by sinusoidal regression (Press, 2002) was done using cross correlation between the interval lengths of 700 kyr and 990 kyr with lag length of 0.1 kyr. The 405 kyr eccentricity cycle could not significantly fit variation of limestone thickness in all intervals as demonstrated by low correlation coefficients with high probability of non-correlation ($p(t) > 0.156$). Nevertheless, a local optimum is located at 779 kyr indicating a precession cycle of exactly 19.0 kyr (Fig. 11A). Much better and highly significant results ($p(t) < 0.01$) are obtained fitting marl thicknesses by sinusoidal regression with fixed period length of 405 kyr. A distinct global optimum is present at an interval of 827 kyr corresponding to a precession period of 20.17 kyr (Fig. 11B). Therefore, both optima differ significantly, and, consequently, we used a combination of limestone and marl data to obtain a better and more stable value for the cycles.

Searching for the best fit based on both variables combines limestone and marls which cannot be directly combined because of different dimensions (limestone thickness: mean = 33.93 cm, standard deviation SD = 18.02; marl thickness: mean = 7.33 cm, SD = 6.52) and the significant negative correlation ($r = -0.2440$, $p(t) = 0.019$) between both variables explained above. Therefore, both parameters were standardized to exclude size differences, and the marl values were subtracted from limestone values due to the

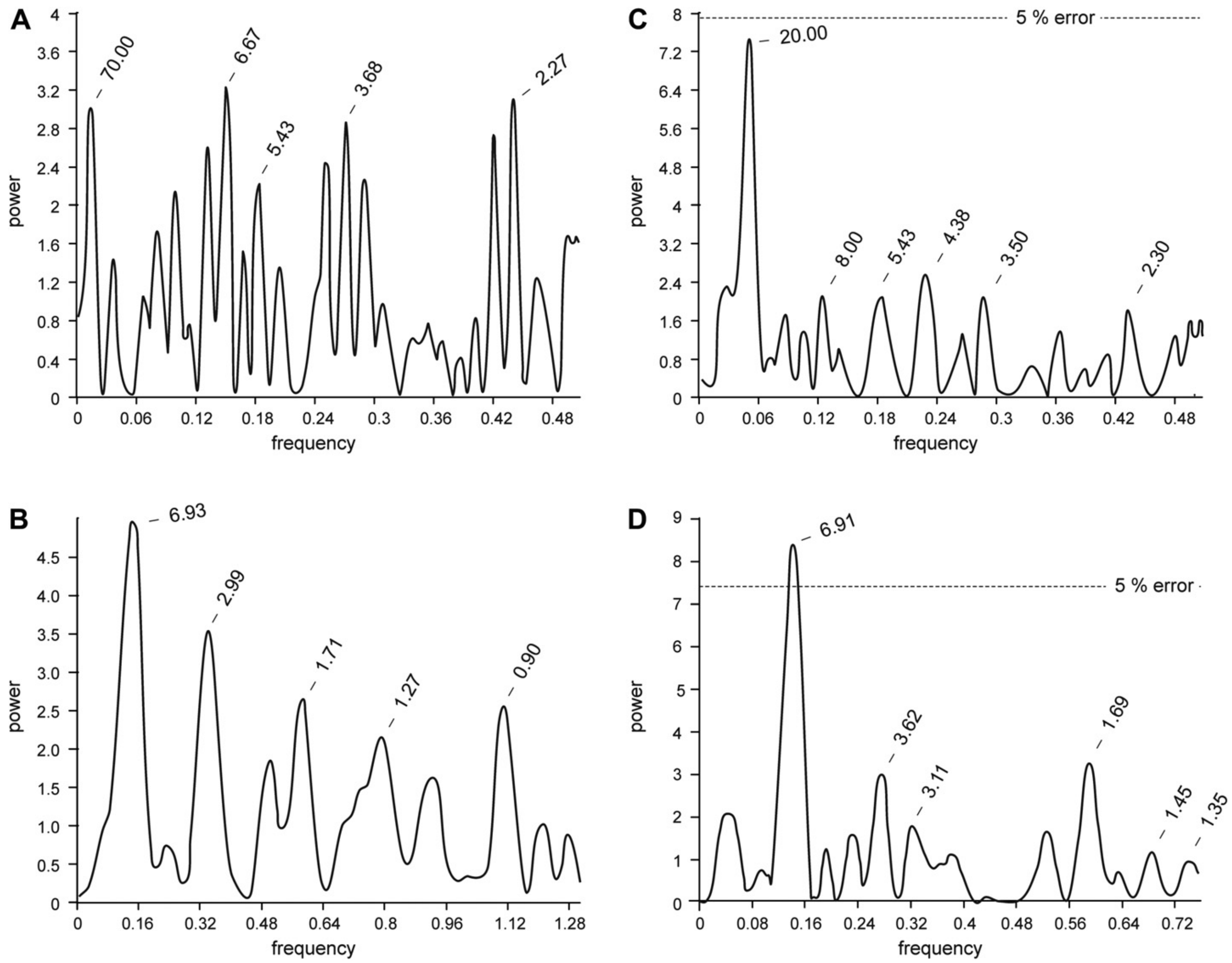

Fig. 8. Power spectra based on the Lomb periodogram algorithm. A. Thickness of limestones per cycle. B. Stable carbon isotopes of limestones. C. Thickness of marls per cycle. D. Stable carbon isotopes of marls. Period lengths indicated by peaks represent number of layers in thickness measures and meters in stable carbon isotopes.

negative correlation. The resulting combined character is characterized by the distribution parameters mean = 0 and SD = 1.577.

Using cross correlation based on sinusoidal regression of the 405 kyr cycle, the optimum was obtained at 806.3 kyr, thus fixing the length of the precession cycle at 19.67 kyr (Fig. 11C). This must not be regarded as a point estimation as long as all correlations based on sinusoidal regression between 17.2 kyr and 22 kyr are significant at the 1% error level (Fig. 11C).

The search for all significant periods in this 806.3 kyr interval was done by "blind" spectral analysis extracting automatically the most significant sinusoidal cycles in decreasing order (Hammer et al., 2001). The results of this automatic analysis are shown in Fig. 11D. The most important period is the automatically fitted 405 kyr cycle, followed by a 107.2 kyr cycle period corresponding to eccentricity 2. The next cycle with period length of 84.17 kyr could be related to the weak peaks at 77, 83 and 88 kyr of the spectral analyses for the last 10 Myr (Hinnov, 2004). The following significant cycle with period length of 236.8 kyr corresponds to the weak peaks between 179 and 220 kyr in spectral analysis of the last 10 Myr (Hinnov, 2004), while the last significant cycle with a period of 39.87 kyr significantly belongs to the group of obliquity cycles with 39.5, 40.2 and 41.0 kyr periods in the late Neogene.

This assumption is corroborated by the identification of corresponding longer cycles ("bundles") and nearly similar results for this zone of 790–800 kyr obtained by Hennebert et al. (2009), Robaszynski and Mzoughi (2010) and Odin (2010).

"Blind" spectral analysis was also used to detect cycles in stable carbon isotopes measured in marls of the Postalm section after transferring section meters restricted to the *calcarata*-zone into time. Resolution is not as good as for the limestone–marl sequences in case of lower sample numbers (39 versus 72). With period lengths of 416, 295.7, 110.1 and 78.66 kyr (Fig. 12A) the estimated periods are extremely similar to periods obtained by the limestone/marl thickness cycles, thus strengthening the correctness of period estimation of orbital cycles for the *calcarata* Zone.

Blind spectral analysis of marl thickness of the whole transect shows similar results with period lengths of 396.7, 236.8, 106.0 and 85.3 kyr (Fig. 12C). In comparison with spectral analysis based on stable carbon isotopes, the significant 45.16 kyr cycle corresponding to obliquity is not figured.

A lowpass filter (Hammer and Harper, 2006) extracting the 405 kyr cycle of marl thickness shows the same position as the cycle with 405 kyr period obtained by sinusoidal regression (Fig. 12D). Due to unequal distances in stable carbon isotope

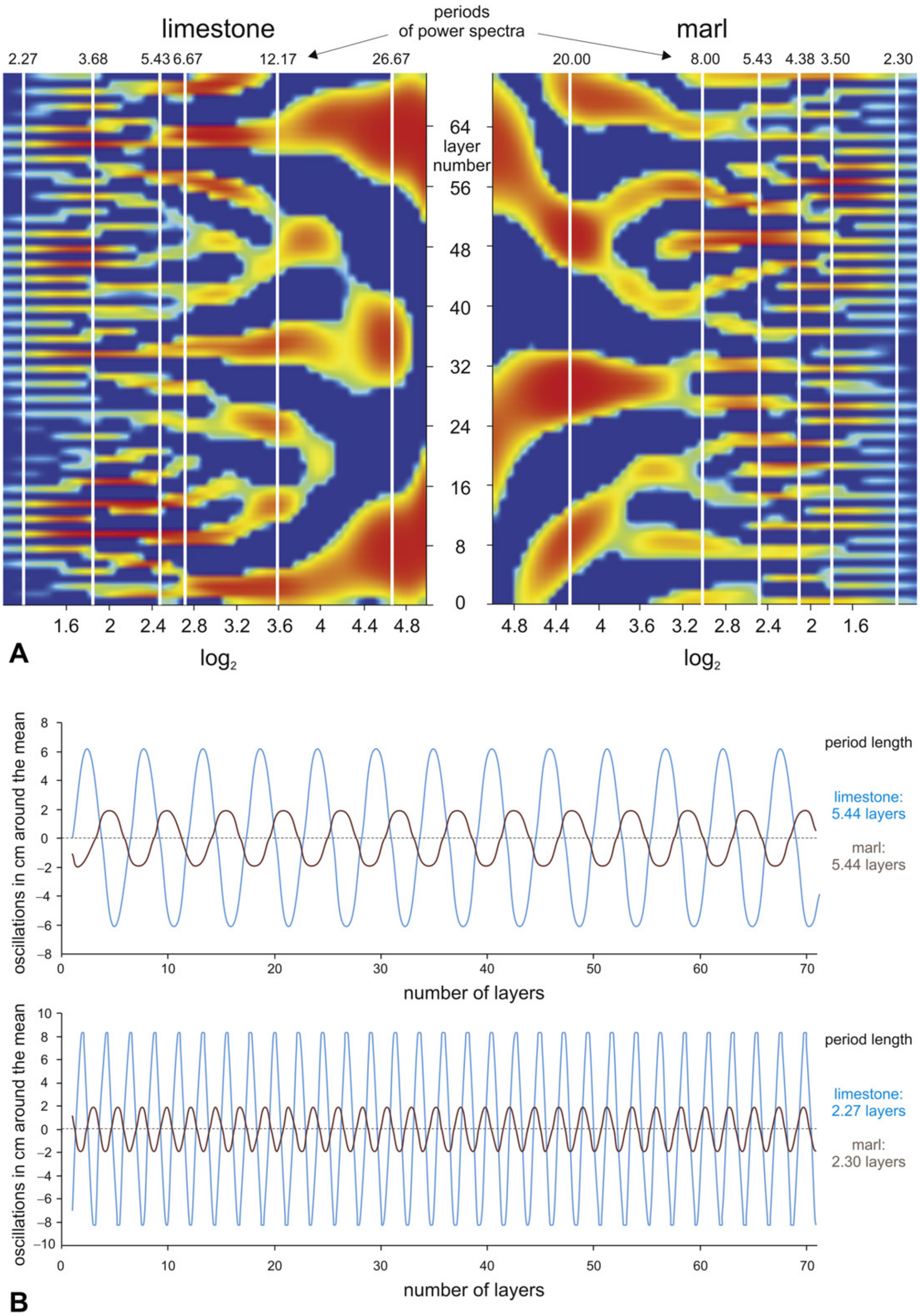

Fig. 9. A. Morlet wavelet analyses for limestone and marl thickness, including the position of peaks obtained by power spectral analysis. B. Alternating thickness oscillations between limestone and marls in sinusoidal functions with equal periods (5.44 layers) and slightly different periods (2.77 versus 2.30 layers).

samples of marls, filtering was impossible, but sinusoidal regression based on the 405 kyr cycle could be performed (Fig. 12B).

Comparing positions of the significant 405 kyr cycles between thickness and stable carbon isotopes of marls, phase differences are visible due to the later onset in thickness (phase 2.86) compared to stable carbon isotopes (phase = 0.364). The coincidence of oscillations in marl thickness and stable carbon isotopes and phase differences could be measured using cross correlation. Cross correlation and their significance based on positive correlations are shown in Fig. 12E. The highest correlation except the large lags

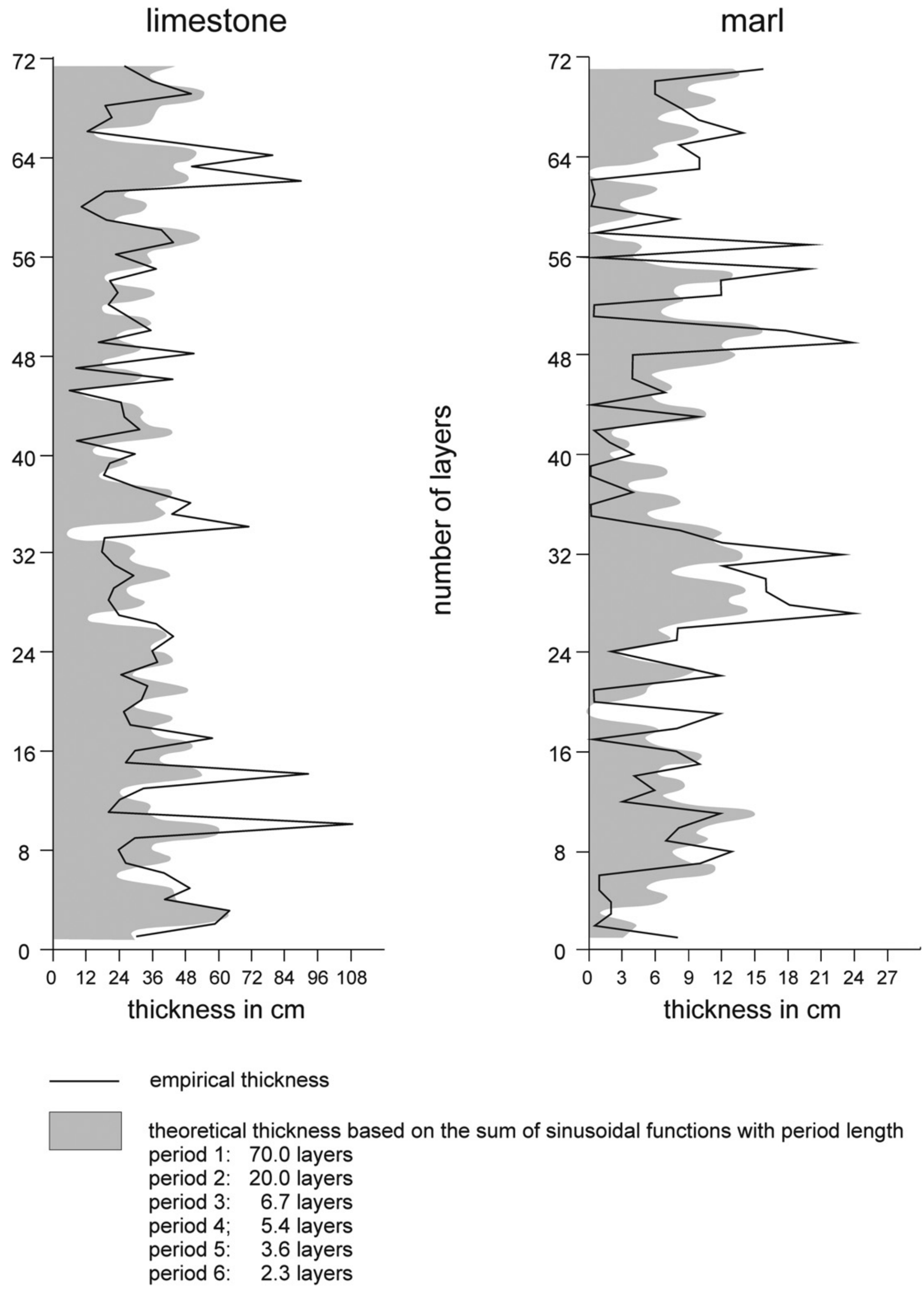

Fig. 10. Fit of empirical thickness in limestones and marls by the sum of 6 sinusoidal functions with identical periods in layer numbers.

at −16 and −15 are at lag +1 ($r = 0.4956$, $p(t) = 0.0182$) corresponding to a time difference of one precession cycle (19.67 kyr) between carbon isotopes and thickness.

The comparison of cycles based on thickness of limestones and their stable carbon content is not as good as for marls. While in blind spectral analysis of the stable carbon isotope content the dominant cycle approximates with 352.2 kyr the 405 kyr cycle, followed by a 89.9 kyr and 102.5 kyr cycle (Fig. 13A), in blind spectral analysis of limestone thickness the largest cycle is missing. But the significant cycles with period lengths in decreasing importance of 44.95 kyr, 107.8 kyr, 79.4 kyr and 244.3 kyr (Fig. 13C) correlate with the shorter cycle periods obtained by the combined limestone/marl thicknesses (Fig. 11D). Fitting the stable carbon isotopes of limestones with the single 405 kyr cycle (Fig. 13B) shows the coincidence with the carbon cycle in marls (Fig. 12B).

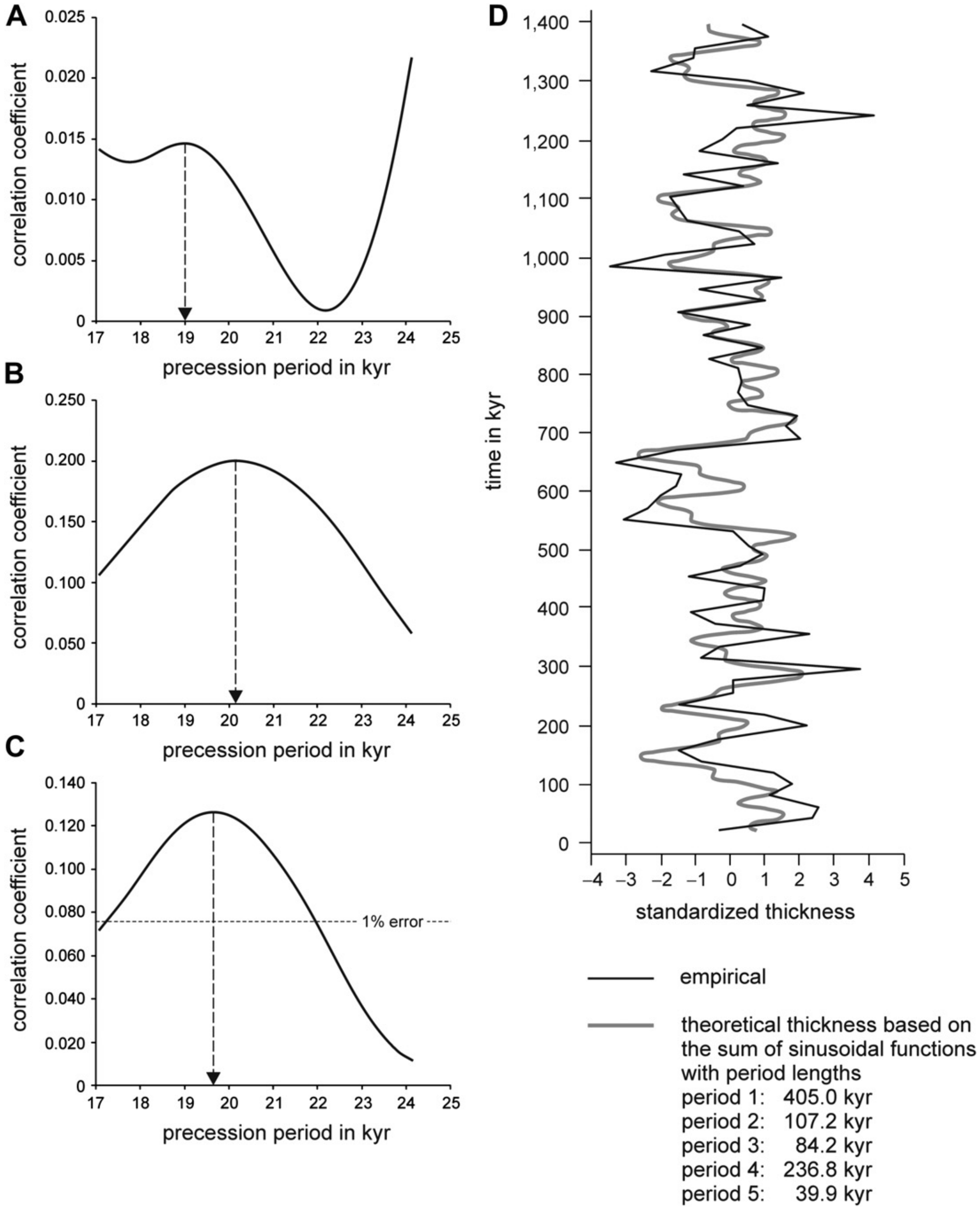

Fig. 11. A–C. Correlograms based on cross correlation between the sinusoidal fit of the 405 kyr eccentricity cycle and time intervals based on precession cycles between 17 kyr and 24 kyr. A. Thickness of limestones. B. Thickness of marls. C. Standardized limestone thickness − standardized marl thickness. D. Fit of the standardized limestone–marl thickness based on the 19.67 kyr precession cycles using blind spectral analysis.

Finally, the correlation of a single limestone/marl cycle with a precession cycle of 19.7 kyr allows the direct transfer of periods, obtained by power spectral analysis of cycle numbers, into time, again strengthening the main orbital cycles in comparison with cycle periods of the last 10 myrs (Table 2).

5. Discussion

5.1. Stable isotope stratigraphy

We compare stable carbon isotope values to the composite stable carbon isotope reference curve of Jarvis et al. (2006) and to the El Kef curve (Jarvis et al., 2002; Fig. 5). Carbon isotope variations in the Trunch borehole were used to correlate the TRZ of *R. calcarata* into the chalk composite curve. During the Campanian, Trunch was situated at the north of the East Anglian island and had boreal influences (Jarvis et al., 2002). El Kef and other nearby Tunisian sections are Tethyan sections with a very high sediment accumulation rate located at the northern margin of the African shelf. The *calcarata* zone shows thicknesses up to 80 m, e.g., at Kalaat Senan (Robaszynski et al., 2000), compared to 16.04 m at the Postalm section.

In general, the *calcarata* Zone is situated above the mid-Campanian carbon isotope event of Jarvis et al. (2002), a significant positive carbon isotope excursion within nannofossil zone CC21, and below the Late (or Upper) Campanian event (Fig. 4), a significant negative carbon isotope excursion in the upper part of nannofossil zone CC22/23a (Jarvis et al., 2002, 2006; Voigt et al.,

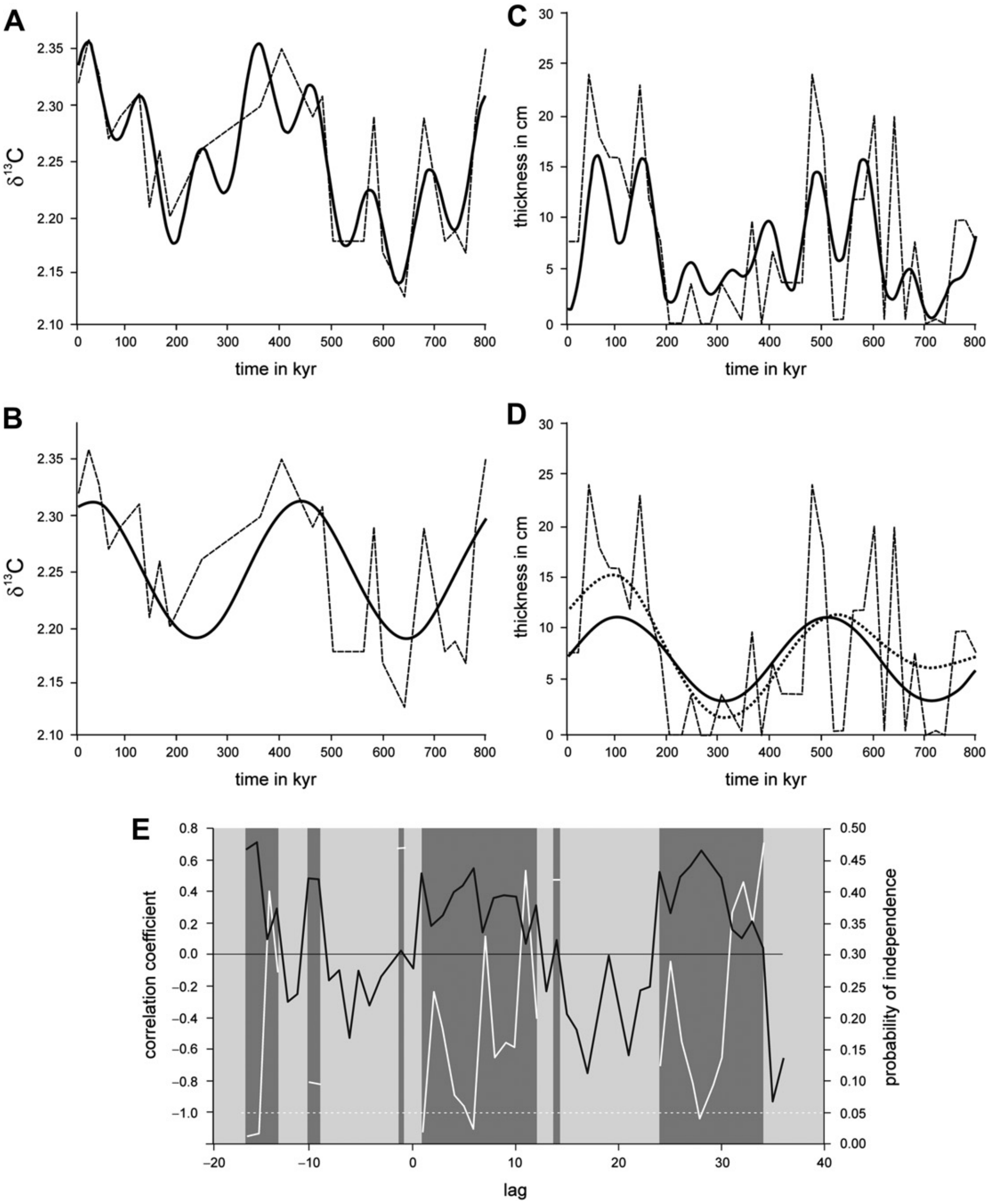

Fig. 12. A–D. Fit of marl measures by blind spectral analysis over the time interval of 806.3 kyr restricted to the *calcarata*-zone. A. Stable carbon isotopes fitted with periods 416 kyr, 295.7 kyr, 110.1 kyr and 78.66 kyr. B. Stable carbon isotopes fitted with period 405 kyr. C. Bed thickness fitted with periods 396.7 kyr, 236.8 kyr, 106.0 kyr and 85.3 kyr. D. Bed thickness fitted with sinusoidal period 405 kyr (black line) and the corresponding lowpass filter (dotted line). E. Cross correlation between thickness and stable carbon isotopes of marls (lag = 19.67 kyr). Black line: Correlation coefficient, white line: probability of independence (non-correlation) in positive correlations.

2010). A slight overall decrease in δ^{13}C within the *calcarata* TRZ (Fig. 5) can be observed in all sections. The Trunch record shows this with little fluctuations compared to Postalm and El Kef. El Kef has on average 0.5‰ less δ^{13}C compared to Postalm but the peak sizes and δ^{13}C variations are largely similar.

At the Postalm section and in the sections of Jarvis et al. (2002), three minor (<5‰) carbon isotope excursions ("events") can be recognized and tentatively correlated: (1) a positive excursion at the onset of the *calcarata* Zone and thus at the onset of CC22a/ UC15de^{TP} ("Calcarata 1 event", c1 in Fig. 5); (2) a positive excursion in the middle part of the *calcarata* Zone ("Calcarata 2 event", c2 in Fig. 5); and (3) a positive excursion right at the end of the *calcarata* Zone ("Calcarata 3 event", c3 in Fig. 5). In addition, slightly below the FO of *R. calcarata* (and *Uniplanarius (Quadrum) trifidus*), a negative excursion can be correlated to the Tunisian sections of Jarvis et al. (2002) and to Tibetian sections (Wendler et al., 2011). In principle, these minor events can be also found in the Pacific, at Shatsky Rise, below the Late Campanian Event (Voigt et al., 2010). Our c1 event can be correlated with the upper part of the Base Calcarata Event of Wendler et al. (2011).

5.2. Duration of the calcarata Zone based on orbital cyclicity

The duration of the *calcarata* Zone is commonly estimated between 500 kyr and a maximum of 1.5 myr. Up to now no direct geochronological dating exists, and correlations to

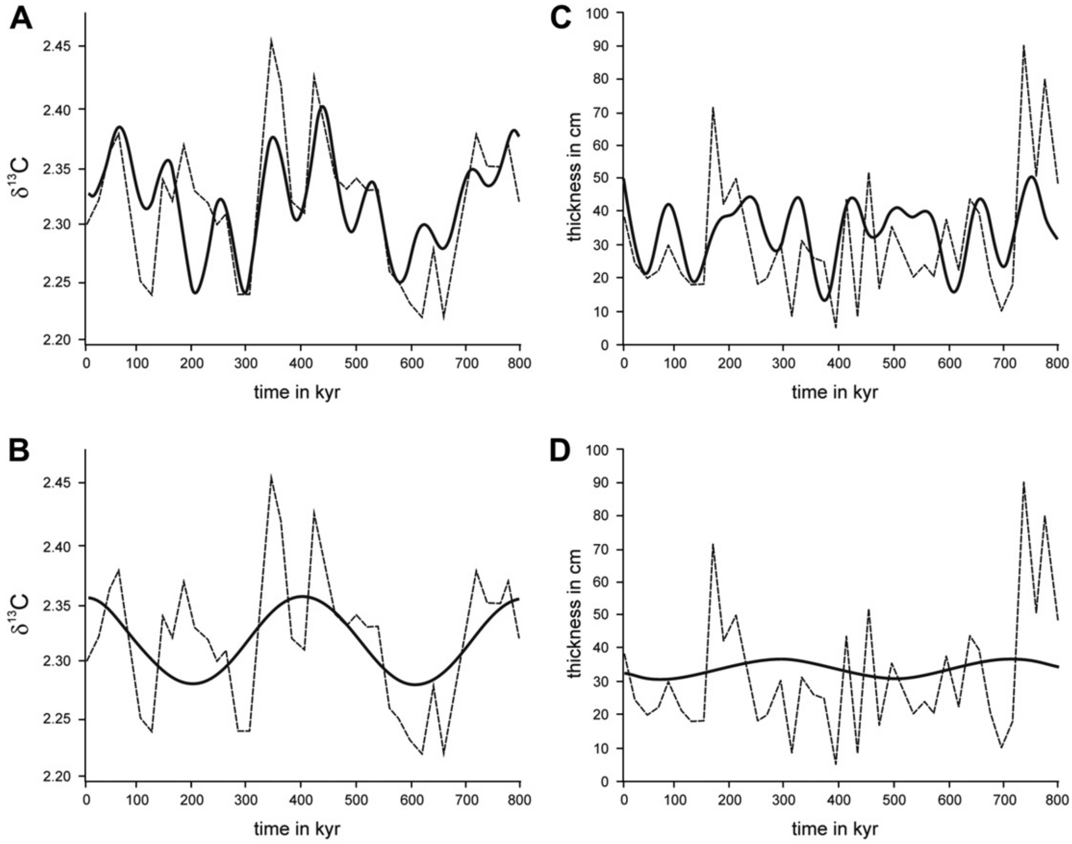

Fig. 13. A–D. Fit of limestone measures by blind spectral analysis over the time interval of 806.3 kyr restricted to the *calcarata*-zone. A. Stable carbon isotopes fitted with periods 352.2 kyr, 89.9 kyr, and 102.5 kyr. B. Stable carbon isotopes fitted with period 405 kyr. C. Bed thickness fitted with periods 107.8 kyr, 79.4 kyr, and 244.3 kyr. D. Bed thickness fitted with period 405 kyr.

geochronologically dated bentonite/tuff bearing sections are only established indirectly, via other fossil markers. Robaszynski and Caron (1995: 1 Ma, 76.7–75.7 Ma), Hardenbol et al. (1998: 0.99 Ma, 76.20–75.21 Ma), and Ogg et al. (2004: 0.7 Ma, 76.3–75.6 Ma) indicate a duration of between 0.7 and 1 myr. A duration of 500 kyr was reported by Caron (1985) and by the ODP/IODP Cretaceous planktic foraminifer datums (e.g., Huber et al., 2008: 75.57–75.07 Ma). Data given by Jarvis et al. (2002: 1.8 myr, 77.0–75.2 Ma) differ considerably, probably because of the unusual thickness of the *calcarata* Zone in Tunisia (Nederbragt, 1991) and problems in correlating carbon isotope excursions from the English chalk to Italian sections (see also Wagreich et al., 2009b).

More recent data were provided by Hennebert et al. (2009) and Robaszynski and Mzoughi (2010) from the Ellès section of Tunisia, and a compilation by Odin (2010) based on Tercis and related sections in France, Tunisia and Spain. At Tunisia, a cyclic record of the Late

Table 2
Transfer of period lengths of power spectra into age and their correspondence to orbital cycles.

Limestone thickness			Marl thickness		
Period length			Period length		
Number of layers	Transfer to kyr	Corresponding orbital cycle	Number of layers	Transfer to kyr	Corresponding orbital cycle
70.00	1,377		20.00	393.3	405,000
6.67	131.1	127,000	8.00	157.3	127,000
5.43	106.8	97,000	5.44	106.9	97,000
3.68	72.5	77,000	4.38	86.0	77,000
2.27	44.6	41,000	*3.50*	68.8	
			2.30	45.3	41,000
Limestone δ^{13}C			Marl δ^{13}C		
Period length			Period length		
Meter	Transfer to kyr	Corresponding orbital cycle	Meter	Transfer to kyr	Corresponding orbital cycle
6.93	402,888	405,000	6.91	401,697	405,000
2.99	173,977		3.62	210,440	
1.71	99,415	97,000	3.11	180,793	
1.27	73,828	77,000	1.69	98,244	97,000
0.90	52,433	41,000	1.45	84,292	
			1.35	78,479	77,000

Campanian including the *calcarata* Zone was interpreted in detail by Hennebert et al. (2009). Based on the extended record at Ellès, i.e. more than 30 m total range of *R. calcarata*, Robaszynski and Mzoughi (2010) calculated a mean duration of the *calcarata* Zone of 790–830 kyr based on two different age estimates by using either precession (20 kyr resulting in 830 kyr) or short eccentricity (100 kyr resulting in 790 kyr) cycles of Hennebert et al. (2009). A nearly similar estimate of the duration of the *calcarata* Zone of 800 $\pm$ 50 kyr was given by Odin (2010) using several correlated sections including the GSSP at Tercis (France) and ultimately based on the data of Hennebert et al. (2009). These durations are, within the error ranges, similar to our calculations which resulted in a duration of 806.3 kyr based on combined marl and limestone cycles.

5.3. Sediment accumulation rates

The average sediment accumulation rate at the Postalm section during the *calcarata* Zone is 1.99 cm/kyr and thus compares well to the sediment accumulation rate of the whole Campanian CORBs in this section (Wagreich and Krenmayr, 2005: 2.6 cm/kyr; Scott, 2009: 1.88 cm/kyr).

5.4. Chronostratigraphic implications

Implications for chronostratigraphy and the geological time scale can be discussed using published data and our new results. The *calcarata* Zone is generally positioned within Magnetochron C33n, from C33n.76 to C33n.92 (i.e. 76%–92% above the base of C33n according to Premoli Silva and Sliter, 1994, and Huber et al., 2008). Ogg et al. (2004) indicated the base of the *calcarata* Zone at 76.18 Ma and the top at 75.57 Ma. Huber et al. (2008) modified that to 75.57 Ma for the base and 75.07 for the top of the zone. The most recent GTS time scale uses c. 75.57 Ma for the base and c. 74.47 Ma for the top of the *calcarata* Zone (TSCreator, Version 5.3; January 2012, http://www.tscreator.org) and the top of C33n at 73.6 Ma. Correlation by carbon isotope stratigraphy (Jarvis et al., 2002, 2006) resulted in ages of c. 77–75.2 Ma and thus a considerable longer time interval. The compilation by Odin (2010) indicates an age of the *calcarata* Zone of 74.3–75.1 Ma.

As mentioned above, no direct geochronological dating of the *calcarata* Zone is available. Published astrochronological calibrations are only based on a floating time scale; however, the most recent two solutions for the top of chron C33n down from the K/Pg boundary give an age of c. 74.2 or 73.8, and thus differ in one 405 kyr cycle (Husson et al., 2011). Extrapolating the top of the *calcarata* Zone from the Ogg et al. (2004) time scale (top of C33n at 73.6 Ma) using adapted tops of chron C33n as indicated by Husson et al. (2011) may thus give an age of the top of the *calcarata* Zone at either 75.1 Ma (solution 1) or 74.7 Ma (solution 2) and, based on the duration of 0.806 Myr of the zone as indicated by Robaszynski and Mzoughi (2010) and refined in this paper, an age of the base of the *calcarata* Zone at either 74.3 Ma (solution 1) or 73.9 Ma (solution 2). Although these ages are still loosely defined, the need for recalibration of the geological time scale is evident and future astronomical tuning will result in more accurate and precise age dates for the *calcarata* Zone and the whole Campanian.

6. Conclusion

Based on the identification of *Radotruncana* (*Globotruncanita*) *calcarata* in the cyclic Postalm section of the Northern Calcareous Alps, we were able to count 41 marl–limestone couplets in the *calcarata* Zone. Cyclicity was determined by the variation in thickness of limestone and marl beds. Results from Sr isotope stratigraphy are in accordance with the temporal position. Further, we related stable carbon isotope excursions to section meters. Orbital cycles were identified and confirm a precessional origin of the limestone–marl cycles and the presence of the long and stable 405 kyr eccentricity cycle, thus indicating a duration of c. 806 kyr for the *calcarata* Zone, in accordance with previous data by Robaszynski and Mzoughi (2010). Based on correlations an age of the top of the *calcarata* Zone at either 75.1 Ma or 74.7 Ma and an age of the base of the *calcarata* Zone at either 74.3 Ma or 73.9 Ma is concluded.

Acknowledgments

Field work was covered by IGCP 555 grants of the Austrian Academy of Sciences and the Austrian Science Fund (FWF): P24044-N24. S.N. was funded by a DocFForte grant for PhD students of the Austrian Academy of Sciences and by a research scholarship from the University of Vienna. We are grateful for the help of Christoph Spötl and Manuela Wimmer (Institute of Geology and Paleontology, University of Innsbruck) with ICP-MS and stable isotope measurements. We thank Monika Horschinegg (Department of Lithospheric Research, Center for Earth Sciences, University of Vienna) for strontium isotope analysis. This is a contribution to IGCP project IGCP 555.

References

Agterberg, F.P., Banerjee, I., 1969. Stochastic model for the deposition of varves in glacial Lake Barlow, Ojibway, Ontario, Canada. Canadian Journal of Earth Sciences 6, 625–652.

Anderson, T.F., Arthur, M.A., 1983. Stable isotopes of oxygen and carbon and their application to sedimentologic and paleoenvironmental problems. In: Arthur, M.A., Anderson, T.F., Kaplan, I.R., Veizer, J., Land, L.S. (Eds.), Stable Isotopes in Sedimentary Geology. SEPM Short Course 10, Tulsa, pp. 1.1–1.151.

Burnett, J.A., 1998. Upper Cretaceous. In: Brown, P.R. (Ed.), Calcareous Nannofossil Biostratigraphy. Chapman & Hall, Cambridge, pp. 132–199.

Berger, A., Loutre, M.F., Laskar, J., 1992. Stability of the astronomical frequencies over the Earth's history fore paleoclimate studies. Science 255, 560–566.

Caron, M., 1985. Cretaceous planktonic foraminifera. In: Bolli, H.M., Saunders, J.B., Perch-Nielsen, K. (Eds.), Plankton stratigraphy. Cambridge University Press, Cambridge, pp. 17–86.

Cushman, J.A., 1927. New and interesting foraminifera from Mexico and Texas. Contributions from the Cushman Laboratory for Foraminiferal Research 3 (41), 1–115.

Egger, H., Mohammed, O., 2010. A slope-basin model for early Paleogene deep-water sedimentation (Achthal Formation nov. nom.) at the Tethyan continental margin (Ultrahelvetic realm) of the European Plate (Eastern Alps, Germany). Austrian Journal of Earth Sciences 103, 121–137.

Faupl, P., Wagreich, M., 2000. Late Jurassic to Eocene palaeogeography and geodynamic evolution of the Eastern Alps. Mitteilungen der Österreichischen Geologischen Gesellschaft 92, 79–94.

Gale, A.S., Hancock, J.M., Kennedy, W.J., Petrizzo, M.R., Lees, J.A., Walaszczyk, I., Wray, D.D., 2008. An integrated study (geochemistry, stable oxygen and carbon isotopes, nannofossils, planktonic foraminifera, inoceramid bivalves, ammonites and crinoids) of the Waxachachie Dam Spillway section, north Texas: a possible boundary stratotype for the base of the Campanian stage. Cretaceous Research 29, 131–167.

Gardin, S., Odin, G.S., Bonnemaison, M., Melinte, C., Monechi, S., von Salis, K., 2001. Results of the cooperative study on the calcareous nannofossils across the Campanian–Maastrichtian boundary at Tercis les Bains (Landes, France). In: Odin, G.S. (Ed.), The Campanian–Maastrichtian Boundary. Elsevier Science, Amsterdam, pp. 293–309.

Hammer, Ø., Harper, D.A.T., 2006. Paleontological data analysis. Blackwell Publishing, Malden, 351 pp.

Hammer, Ø., Harper, D.A.T., Ryan, P.D., 2001. PAST: Palaeontological Statistics software package for education and data analysis. Palaeontologia Electronica 4 (1), 9 pp.

Hardenbol, J., Thierry, J., Farley, M.B., Jacquin, T., de Graciansky, P.-C., Vail, P.R., 1998. Mesozoic and Cenozoic sequence chronostratigraphic framework in European basins. In: de Graciansky, P.-C., Hardenbol, J., Jacquin, T., Vail, P.R. (Eds.). Mesozoic and Cenozoic Sequence Stratigraphy of European Basins, 60. SEPM Special Publication, pp. 3–13.

Hennebert, M., Robaszynski, F., Goolaerts, S., 2009. Cyclostratigraphy and chronometric scale in the Campanian – Lower Maastrichtian: the Abiod Formation at Ellès, central Tunisia. Cretaceous Research 30, 325–338.

Herbert, T.D., Gee, J., DiDonna, S., 1999. Precessional cycles in Upper Cretaceous pelagic sediments of the South Atlantic: Long-term patterns from high-frequency climate variations. In: Barrera, E., Johnson, C.C. (Eds.). Evolution of the Cretaceous Ocean-Climate System, 332. Geological Society of America Special Paper, pp. 105–120.

Hinnov, L.A., 2004. Earth's orbital parameters and cycle stratigraphy. In: Gradstein, F., Ogg, J., Smith, A. (Eds.), A Geologic Time Scale 2004. Cambridge University Press, pp. 55–62.

Hinnov, L.A., Ogg, J.G., 2007. Cyclostratigraphy and the Astronomical Time Scale. Stratigraphy 4, 239–251.

Hohenegger, J., Wagreich, M., 2012. Time calibration of sedimentary sections based on insolation cycles using combined cross-correlation: dating the gone Badenian stratotype (Middle Miocene, Paratethys, Vienna Basin, Austria) as an example. International Journal of Earth Sciences 101, 339–349.

Hu, X., Jansa, L., Wang, C., Sarti, M., Bak, K., Wagreich, M., Michalik, J., Soták, J., 2005. Upper Cretaceous oceanic red beds (CORBs) in the Tethys: occurrences, lithofacies, age, and environments. Cretaceous Research 26, 3–20.

Huber, B.T., Norris, R.D., MacLeod, K.G., 2002. Deep-sea paleotemperature record of extreme warmth during the Cretaceous. Geology 30, 123–126.

Huber, B.T., MacLeod, K.G., Tur, A.N., 2008. Chronostratigraphic framework for upper Campanian–Maastrichtian sediments on the Blake Nose (Subtropical North Atlantic). Journal of Foraminiferal Research 38, 162–182.

Husson, D., Galbrun, B., Laskar, J., Hinnov, L.A., Thibault, N., Gardin, S., Locklair, R.E., 2011. Astronomical calibration of the Maastrichtian (Late Cretaceous). Earth and Planetary Science Letters. doi:10.1016/j.epsl.2011.03.008.

Ion, J., Odin, G.S., 2001. Planktonic foraminifera from the Campaniane Maastrichtian at Tercis les Bains (Landes, France). In: Odin, G.S. (Ed.), The Campanian–Maastrichtian Boundary. Developments in Palaeontology and Stratigraphy, 19, pp. 349–378.

Jarvis, I., Mabrouk, A., Moody, R.T.J., de Cabrera, S., 2002. Late Cretaceous (Campanian) carbon isotope events, sea-level change and correlation of the Tethyan and Boreal realms. Palaeogeography, Palaeoclimatology, Palaeoecology 188, 215–248.

Jarvis, I., Gale, A.S., Jenkyns, H.C., Pearce, M.A., 2006. Secular variation in Late Cretaceous carbon isotopes: a new $\delta^{13}C$ carbonate reference curve for the Cenomanian–Campanian (99.6–70.6 Ma). Geological Magazine 143, 561–608.

Küchler, T., Kutz, A., Wagreich, M., 2001. The Campanian–Maastrichtian boundary in Northern Spain (Navarra province): the Imiscoz and Erro sections. In: Odin, G.S. (Ed.), The Campanian–Maastrichtian Stage Boundary. Developments in Palaeontology and Stratigraphy, 19, pp. 723–744.

Jenkyns, H.C., 2003. Evidence for rapid climate change in the Mesozoic-Palaeogene greenhouse world. Philosophical Transactions of the Royal Society, Series A 361, 1885–1916.

Laskar, J., Fienga, A., Gastineau, M., Manche, H., 2011. La2010: a new orbital solution for the long-term motion of the Earth. Astronomy and Astrophysics 532, A89. doi:10.1051/0004-6361/201116836.

Li, L., Keller, G., Stinnesbeck, W., 1999. The Late Campanian and Maastrichtian in northwestern Tunisia: paleoenvironmental inferences from lithology, macrofauna and benthic foraminifera. Cretaceous Research 20, 231–252.

Longoria, J.F., VonFeldt, A.E., 1991. Taxonomy, phylogenetics and biochronology of single-keeled globotruncanids (Genus *Globotruncanita* Reiss). Micropaleontology 37, 197–243.

McArthur, J.M., Howarth, R.J., 2004. Strontium isotope stratigraphy. In: Gradstein, F.M., Agterberg, F.P., Smith, A.G. (Eds.), A Geologic Time Scale 2004. Cambridge University Press, Cambridge, pp. 96–105.

McArthur, J.M., Howarth, R.J., Bailey, T.R., 2001. Strontium isotope stratigraphy: LOWESS Version 3: best fit to the marine Sr-isotope curve for 0–509 Ma and accompanying look-up table for deriving numerical age. Journal of Geology 109, 155–170.

Nederbragt, A.J., 1991. Late Cretaceous biostratigraphy and development of Heterohelicidae (planktic foraminifera). Micropaleontology 37, 329–372.

Neuhuber, S., Wagreich, M., 2009. The Late Campanian Globotruncanita calcarata Zone (Ultrahelvetics, Austria): implications from nannofossil stratigraphy, stable isotopes and geochemistry. Abstracts 8th International Symposium on the Cretaceous System, Univ. Plymouth, 6th–12th September 2009, p. 91.

Neuhuber, S., Wagreich, M., Wendler, I., Spötl, C., 2007. Turonian Oceanic Red Beds in the Eastern Alps: concepts or palaeoceanographic changes in the Mediterranean Tethys. Palaeogeography, Palaeoclimatology, Palaeoecology 251, 222–238.

Odin, G.S., 2010. Traces de volcanisme explosif dans le Campanien pyrénéen aux alentours du stratotype de limite Campanien-Maastrichtien à Tercis (SO France, N Espagne). Repérage biostratigraphique avec une étude particulière du foraminifère *Radotruncana calcarata*. Carnets de Géologie/Notebooks on Geology, 2010/02 (CG2010_A02), 35 pp.

Odin, G.S., Gardin, S., Robaszynski, F., Thierry, J., 2004. Stage boundaries, global stratigraphy, and the time scale: towards a simplification. Carnets de Géologie 2004/02.

Odin, G.S., Lamaurelle, M.A., 2001. The global Campanian–Maastrichtian stage boundary. Episodes 24, 229–238.

Ogg, J.G., Agterberg, F.P., Gradstein, F.M., 2004. The Cretaceous Period. In: Gradstein, M., Agterberg, F.P., Smith, A.G. (Eds.), A Geologic Time Scale 2004. Cambridge University Press, Cambridge, pp. 344–383.

Perch-Nielsen, K., 1985. Mesozoic Calcareous Nannofossils. In: Bolli, H.M., Saunders, J.B., Perch-Nielsen, K. (Eds.), Plankton Stratigraphy. Cambridge University Press, Cambridge, pp. 329–426.

Petrizzo, R.M., Falzoni, F., Premoli Silva, I., 2011. Identification of the base of the lower-to-middle Campanian *Globotruncana ventricosa* Zone: comments on reliability and global correlations. Cretaceous Research 32, 387–405.

Premoli Silva, I., Spezzaferri, S., d'Angelantonio, A., 1998. Cretaceous foraminiferal bio-isotope stratigraphy of Hole 967E and Paleogene planktonic foraminiferal biostratigraphy of Hole 966F, Eastern Mediterranean. In: Robertson, A.H.F., Emeis, K.-C., Richter, C., Camerlenghi, A. (Eds.). Proceedings of the Ocean Drilling Program, Scientific Results, Vol. 160.

Press, W.H., 2002. Numerical Recipes in C. Cambridge University Press, Cambridge, 994 pp.

Puckett, T.M., Mancini, E.A., 1998. Planktic foraminiferal *Globotruncanita calcarata* Total Range Zone: its global significance and importance to chronostratigraphic correlation in the Gulf Coastal Plain, USA. Journal of Foraminiferal Research 28, 124–134.

Robaszynski, F., Gonzales, J.M., Linares, D., Amédro, F., Caron, M., Dupuis, C., Dhondt, A., Gartner, S., 2000. Le Crétacé Supérieur de la Région de Kalaat Senan, Tunisie Centrale. Lithobiostratigraphie intégrée: zones d'ammonites, de foraminifères planctoniques et de nannofossiles du Turonien supérieur au Maastrichtien. Bulletin des Centres de Recherche Exploration Production Elf-Aquitaine, Pau 22, 359–490.

Robaszynski, F., Caron, M., 1995. Foraminifères planctoniques du Crétacé: commentaire de la zonation Europe-Méditerrané. Bulletin de la Société Géologique de France 166, 681–692.

Robaszynski, F., Mzoughi, M., 2010. The Abiod at Ellès (Tunisia): stratigraphies, Campanian–Maastrichtian boundary, correlation. Carnets de Géologie 2010/4.

Robaszynski, F., Caron, M., Gonzales, J.M., Wonders, A.H. (Eds.). European Working Group on Planktonic Foraminifera, 1984. Atlas of Late Cretaceous globotruncanids. Revue de Micropaléontologie, 26, pp. 145–305.

Schönfeld, J., Burnett, J., 1991. Biostratigraphical correlation of the Campanian–Maastrichtian boundary: Lägerdorf–Henmoor (northwestern Germany); DSDP Sites 548A, 549 and 551 (eastern North Atlantic) with palaeobiogeographical and palaeoceanographical implications. Geological Magazine 128, 479–503.

Schwarzacher, W., 1975. Sedimentation models and quantitative stratigraphy. Elsevier, Amsterdam, 382 pp.

Scott, R.W., 2009. Chronostratigraphic database for Upper Cretaceous oceanic red beds (CORBs). In: Hu, X., Wang, C., Scott, R.W., Wagreich, M., Jansa, L. (Eds.). Cretaceous Oceanic Red Beds: Stratigraphy, Composition, Origins, and Paleoceanographic and Paleoclimatic Significance, 91. SEPM Special Publication, pp. 35–58.

Sigal, J., 1977. Essai de zonation du Crétacé méditerranéen à l'aide des foraminifères planctoniques. Géologie Méditerranéenne 4, 99–108.

Premoli Silva, I., Sliter, W.V., 1994. Cretaceous planktonic foraminiferal biostratigraphy and evolutionary trends from the Bottaccione section, Gubbio, Italy. Palaeontographia Italica 82, 1–89.

Spötl, C., Vennemann, T., 2003. Continuous-flow isotope ratio mass spectrometric analysis of carbonte minerals. Rapid Communications in Mass Spectrometry 17, 1004–1006.

Voigt, S., Schönfeld, J., 2010. Cyclostratigraphy of the reference section for the Cretaceous white chalk of northern Germany, Lägerdorf–Kronsmoor: a late Campanian–early Maastrichtian orbital time scale. Palaeogeography, Palaeoclimatology, Palaeoecology 287, 67–80.

Voigt, S., Friedrich, O., Norris, R.D., Schönfeld, J., 2010. Campanian–Maastrichtian carbon isotope stratigraphy: shelf-ocean correlation between the European shelf sea and the tropical Pacific Ocean. Newsletters on Stratigraphy 44, 57–72.

Wagreich, M., 1993. Subcrustal tectonic erosion in orogenic belts – A model for the Late Cretaceous subsidence of the Northern Calcareous Alps (Austria). Geology 21, 941–944.

Wagreich, M., Hu, X., Sageman, B., 2011. Causes of oxic-anoxic changes in Cretaceous marine environments and their implications for Earth systems. Sedimentary Geology 235, 1–4.

Wagreich, M., Krenmayr, H.-G., 1993. Nannofossil biostratigraphy of the Late Cretaceous Nierental Formation, Northern Calcareous Alps (Bavaria, Austria). Zitteliana 20, 67–77.

Wagreich, M., Krenmayr, H.-G., 2005. Upper Cretaceous oceanic red beds (CORB) in the Northern Calcareous Alps (Nierental Formation, Austria): slope topography and clastic input as primary controlling factors. Cretaceous Research 26, 57–64.

Wagreich, M., Neuhuber, S., Egger, J., Wendler, I., Scott, R.W., Malata, E., Sanders, D., 2009a. Cretaceous oceanic red beds (CORBs) in the Austrian Eastern Alps: passive-margin vs. active-margin depositional settings. In: Hu, X., Wang, C., Scott, R.W., Wagreich, M., Jansa, L. (Eds.). Cretaceous Oceanic Red Beds: Stratigraphy, Composition, Origins, and Paleoceanographic and Paleoclimatic Significance, 91. SEPM Special Publication, pp. 73–88.

Wagreich, M., Summesberger, H., Kroh, A., 2009b. Late Santonian bioevents in the Schattau section, Gosau Group of Austria – implications for the Santonian–Campanian boundary stratigraphy. Cretaceous Research 31, 181–191.

Wendler, I., Willems, H., Gräfe, K.-U., Ding, L., Luo, H., 2011. Upper Cretaceous interhemispheric correlation between the Southern Tethys and the Boreal: chemo- and biostratigraphy and paleoclimatic reconstructions from a new section in the Tethys Himalaya, S-Tibet. Newsletters on Stratigraphy 44, 137–171.

Westphal, H., Munnecke, A., 2003. Limestone–marl alternations: a warm-water phenomenon? Geology 31, 263–266.

Westphal, H., Hilgen, F., Munnecke, A., 2010. An assessment of the suitability of individual rhythmic carbonate successions for astrochronological application. Earth-Science Reviews 99, 19–30.